Available online at www.sciencedirect.com
SCIENCE DIRECT®
Journal of Solid State Chemistry 178 (2005) 2846–2857
JOURNAL OF SOLID STATE CHEMISTRY
www.elsevier.com/locate/jssc

# A combined X-ray diffraction and Raman scattering study of the phase transitions in $Sr_{1-x}Ca_xTiO_3$ ($x = 0.04$, 0.06, and 0.12)

Sanjay Kumar Mishra[a], Rajeev Ranjan[a], Dhananjai Pandey[a,*], Pierre Ranson[b], Robert Ouillon[b], Jean-Paul Pinan-Lucarre[b], Philippe Pruzan[b]

[a]*School of Materials Science and Technology, Institute of Technology, Banaras Hindu University, Varanasi-221005, India*
[b]*Laboratoire de Physique des Milieux Condensés, UMR 7602, Université Pierre et Marie Curie, 140 rue de Lourmel, 75015 Paris, France*

Received 21 February 2005; received in revised form 22 June 2005; accepted 23 June 2005

**Abstract**

Results of powder X-ray diffraction and Raman scattering studies on the phase transitions in $Sr_{1-x}Ca_xTiO_3$ (SCT) are presented for $x = 0.04$, 0.06 and 0.12 in the temperature range 8–473 K. It is proposed that the space group of SCT in the composition range $0.06 \leqslant x \leqslant 0.35$ is *Imma* with $a^0b^-b^-$ tilt system and not $I4/mcm$ with $a^0a^0c^-$ tilt system, as assumed by earlier workers. The lowering of the crystal symmetry from $I4/mcm$ to *Imma* is supported by the observation of additional Raman lines, in agreement with the factor group analysis for the *Imma* space group. The structural $E_g$ mode, characteristics of the non-cubic phase, is shown to be present even in the cubic phases of $x = 0.06$ and $x = 0.12$ but not of $x = 0.04$ indicating the change in the local structure of the cubic phase of SCT for $x \geqslant 0.06$. The presence of symmetry forbidden $TO_2$ mode in the Raman spectra of the cubic phase of SCT for $x < 0.06$ and its absence for $x \geqslant 0.06$ provides yet another characteristic feature distinguishing the $I4/mcm$ and *Imma* space groups. The implications of the change in the tilt system from $a^0a^0c^-$ to $a^0b^-b^-$ on the development of the polar order is also discussed.


*Keywords:* Perovskites; Powder X-ray diffraction; Raman spectra; Phase transition

## 1. Introduction

$SrTiO_3$ is a well-known quantum paraelectric [1]. Its dielectric constant ($\varepsilon'$) increases with decreasing temperature up to about 4 K due to the softening of the zone centre $TO_1$ transverse-optic mode [2,3]. Quantum fluctuations, however, preclude the condensation of this soft mode below 4 K as a result of which the dielectric constant shows saturation below 4 K [1]. $SrTiO_3$ is therefore termed as an incipient ferroelectric down to $T \approx 0$ K. There is also the possibility [4–8] of a quantum phase transition into a coherent quantum state below 36 K similar to that in liquid He II [9].

The presence of substitutional impurities like $Ca^{2+}$, $Ba^{2+}$ and $Pb^{2+}$ at the $Sr^{2+}$ site or $O^{18}$ isotope at the $O^{2-}$ site is known to induce a transition into a polar phase at non-zero temperatures [10–14]. The nature of these transitions depends largely on the concentration and type of impurity. In the $(Sr_{1-x}Ca_x)TiO_3$ (SCT) system, if the $Ca^{2+}$ content is more than a critical value $x_c \approx 0.0018$, it stabilizes X–Y type quantum ferroelectricity [11]. The transition temperature ($T_c$) follows $T_c = (x - x_c)^{0.5}$ type of composition dependence as expected for quantum ferroelectrics [15]. For $0.016 \leqslant x \leqslant 0.12$, the $\varepsilon'$ vs. $T$ plots are smeared out, which was originally attributed to the formation of random field induced ferroelectric domains [11], but could possibly be due to a relaxor ferroelectric or dipole glass type transition as well [16]. In the composition range $0.12 < x < 0.40$, Ranjan et al. [16] have recently shown that the dielectric anomaly is not due to a ferroelectric or dipole glass/relaxor ferroelectric transition but due to an antiferroelectric phase transition. These workers have argued

*Corresponding author. Fax: +91 542 2368707.
*E-mail address:* dpandey@bhu.ac.in (D. Pandey).

0022-4596/$ - see front matter © 2005 Elsevier Inc. All rights reserved.
doi:10.1016/j.jssc.2005.06.036

that the smeared dielectric $\varepsilon'(T)$ response in the composition range $0.016 \leqslant x \leqslant 0.12$ is due to the frustration introduced by the competing ferroelectric instability of the $SrTiO_3$ matrix and the antiferroelectric instability brought about by $Ca^{2+}$ substitution. For low enough $Ca^{2+}$ concentrations ($0.0018 \leqslant x \leqslant 0.016$), the frustration effects are rather weak, and one therefore observes quantum ferroelectric transitions.

The room-temperature structure of $SrTiO_3$ is cubic and it undergoes an antiferrodistortive phase transition below 105 K leading to a tetragonal phase in which the neighbouring $TiO_6$ octahedra are rotated in an antiphase manner about the [001] axis due to the freezing of a zone boundary phonon corresponding to the R symmetry point ($q = \frac{111}{222}$) of the cubic Brillouin zone [17]. The space group of this tetragonal phase is known to be $I4/mcm$ [17]. The room-temperature structure of SCT is also cubic at room temperature for $0 \leqslant x < 0.06$ [18,19]. The powder diffraction patterns recorded at room temperature for the composition range $0.06 \leqslant x \leqslant 0.35$ resemble the powder diffraction pattern of the tetragonal phase (space group $I4/mcm$) of pure $SrTiO_3$ below 105 K. As a result most of the authors [20–23] have proposed the space group $I4/mcm$ for the room-temperature structure of SCT in the composition range $0.06 \leqslant x \leqslant 0.35$. In terms of Glazer's classification [24,25], this structure belongs to the $a^0a^0c^-$ tilt system. Ranjan et al., on the other hand, have proposed [19] a tilt system $a^0b^-b^-$ with *Imma* space group for these compositions on the basis of their phase transition studies [26]. However, it is not possible to make a choice between the $I4/mcm$ and *Imma* space groups purely on the basis of Rietveld analysis of powder diffraction data, since one obtains comparable agreement factors for both the models. Raman scattering technique is a sensitive tool for exploring the crystal symmetries and we show here that it is possible to make a unique and unambiguous choice between $I4/mcm$ and *Imma* space groups using Raman scattering study of SCT compositions as a function of temperature.

In this paper, we present the results of a combined X-ray powder diffraction and Raman scattering studies on phase transitions in three SCT compositions with $x = 0.04$, 0.06 and 0.12 in the temperature ranges 8–300 K, 8–473 K and 8–460 K, respectively. For the sake of completeness, we have also included our earlier Raman scattering results [27] on SCT06 and SCT12 in the temperature range 8–300 K and reanalysed these data in relation to the structural changes revealed by the X-ray diffraction (XRD) studies over the extended temperature range beyond 300 K. The high-temperature (i.e., $T > 300$ K) Raman scattering studies on SCT06 and SCT12 reveal that the $E_g$ line, characteristic of the non-cubic structure, persists even in the cubic phase whereas it disappears in the cubic phase for SCT04. On the other hand, symmetry forbidden first order $TO_2$ and $TO_4$ lines are observed even in the cubic phase of SCT04 but not in the cubic phase of SCT06 and SCT12. For $x < 0.06$, the Raman spectra of the low-temperature non-cubic phase of SCT is shown to be similar to that of the low-temperature tetragonal phase [space group $I4/mcm$] of pure $SrTiO_3$. But, for $x = 0.06$ and 0.12, five additional Raman lines, not expected for the $I4/mcm$ space group, but in agreement with factor group analysis for the *Imma* space group, are observed. It is proposed that the room-temperature structure of SCT for $x = 0.06$ and 0.12 belongs to the orthorhombic *Imma* space group with $a^0b^-b^-$ tilt system and not to the $I4/mcm$ space group with $a^0a^0c^-$ tilt system.

## 2. Experimental

SCT samples were prepared using a conventional solid state thermochemical reaction method, the details of which are given elsewhere [18]. Raman scattering experiments were performed on sintered pellets of ~13 mm diameter, one face of which was polished with diamond paste to give good reflectivity. The low- and high-temperature scattering measurements were carried out with a monochannel Raman double monochromator (Jobin-Yvon) with 514.5 nm excitation from a laser. The laser power at the sample was kept lower than 100 mW and the spectra were recorded in *a* nearly 90° scattering geometry using a low-angle laser excitation. Most part of the room-temperature scattering measurements was performed using a T64000 Jobin-Yvon Horiba confocal spectrometer equipped with a charge-coupled device (CCD). In this case the 514.5 nm laser power excitation before focusing with a 40 × objective was kept lower than 10 mW. In either case the instrumental resolution was $\tilde{\nu} = 2\,cm^{-1}$. For the low-temperature measurements, the samples were mounted in an optical He cryostat from SMC Instruments. Temperature was controlled and monitored using calibrated Si diodes. For the high-temperature measurements, the pellets were inserted in a block of copper equipped with a regulated electric heater and maintained in a nitrogen environment to avoid chemical degradation. We used the softwares Grams and Spectra Max 32 for the Raman data processing.

XRD data were collected using a 18 kW rotating anode (Cu target, $\lambda = 1.5406$ Å) based Rigaku powder diffractometer (RINT 2000/ PC series) operating in the Bragg–Brentano geometry with a low-temperature attachment (12–300 K). The high-temperature XRD studies above 300 K were carried out on a 12 kW rotating anode (Cu target) based Rigaku powder diffractometer (Model D/max-A) fitted with a Rigaku high-temperature attachment. A curved crystal monochromator in the diffraction beam was used for both the low- and high-temperature XRD measurements. The

temperature was stable within $\pm 1$ K during these measurements. All the XRD data were collected at a scan speed of 1° per minute at a step ($\Delta 2\theta$) of 0.02°. Data analysis was carried out using Le-Bail technique [28].

## 3. Results and discussion

### 3.1. X-ray diffraction studies

#### 3.1.1. The I4/mcm vs. Imma space group for SCT

In the SCT system, one of the end members, $SrTiO_3$, has got cubic perovskite structure with *Pm3m* space group, while the other end member, $CaTiO_3$, has got an orthorhombic structure with space group *Pbnm* at room temperature. In the room-temperature phase of $CaTiO_3$, the $TiO_6$ octahedra are titlted in the $a^-a^-c^+$ manner [24,25]. The room-temperature cubic phase of $SrTiO_3$ transforms below 105 K to a tetragonal structure with *I4/mcm* space group in which the octahedra are tilted in the $a^0a^0c^-$ manner [24,25]. As a consequence of the antiphase (−) and inphase(+) tilts in perovskite structures, a series of superlattice reflections appear in the diffraction patterns because of the unit cell doubling. The Miller indices of the superlattice reflections resulting from antiphase tilts are represented by all-odd (o) integers (i.e., ooo type) with respect to a doubled pseudocubic cell, whereas the in-phase tilt gives rise to superlattice reflections whose two Miller indices are odd integers while the third one is an even (e) integer (i.e., ooe type [24,25]). In the low-temperature ($T < 105$ K) phase of $SrTiO_3$, the superlattice reflections are of odd-odd-odd type only whereas in the $CaTiO_3$ structure the superlattice reflections are of odd-odd-odd as well as odd-odd-even types.

Fig. 1 depicts the room-temperature powder XRD patterns of SCT with $x = 0.00$, 0.02, 0.04, 0.05, 0.06 and 0.12 (i.e., ST, SCT02, SCT04, SCT05, SCT06 and SCT12) in the $2\theta$ range 37–56 and 103°–106°. The main perovskite and the superlattice reflections are marked as P and S in this figure. The superlattice peak around $2\theta = 39°$ is observed for SCT06 and SCT12 but not for $x < 0.06$. For $x = 0.06$, the superlattice peak is very weak and is seen only after appropriate zooming, as shown in the small box in Fig. 1(e). The presence of this superlattice peak clearly indicates non-cubic structure of SCT for $x \geqslant 0.06$. Another signature of the non-cubic structure of SCT at room temperature for $x \geqslant 0.06$ is found in the splitting of the high-angle 4 0 0 perovskite peaks as shown in Fig. 1(k and l).

The SCT compositions with $0 < x < 0.06$ transform from cubic (space group *Pm3m*) to tetragonal (space group *I4/mcm*) structure below room temperature in a manner similar to $SrTiO_3$. Figs. 2 and 3 depict the evolution of the XRD patterns recorded at several temperatures below room temperature for SCT with $x =$

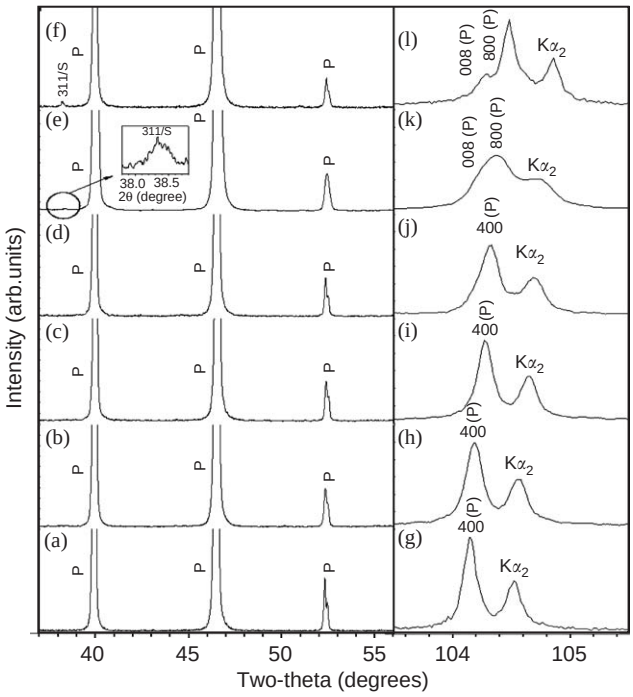


Fig. 1. Room-temperature XRD patterns of $Sr_{1-x}Ca_xTiO_3$ with (a) $x = 0.00$, (b) 0.02, (c) 0.04, (d) 0.05, (e) 0.06 and (f) 0.12 in the $2\theta$ range 37°–56°. The patterns (g)–(l) show the profile shape of the perovskite reflection 4 0 0. The indices in (e), (f), (k) and (l) are with respect to a doubled pseudocubic cell. The inset in (e) shows the superlattice reflection for $x = 0.06$ at room temperature.

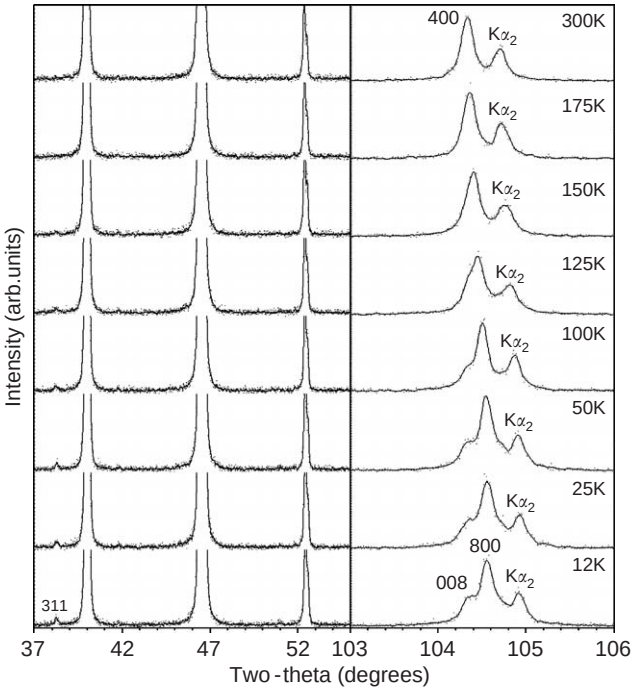


Fig. 2. Evolution of the powder XRD pattern of $Sr_{0.98}Ca_{0.02}TiO_3$ (SCT02) with temperature in the $2\theta$ range 37°–56°. The right hand side block depicts the evolution of the 4 0 0 perovskite reflection which splits into 008 and 800 for $T < 175$ K. The indices are with respect to the doubled pseudocubic cell for $T < 175$ K.

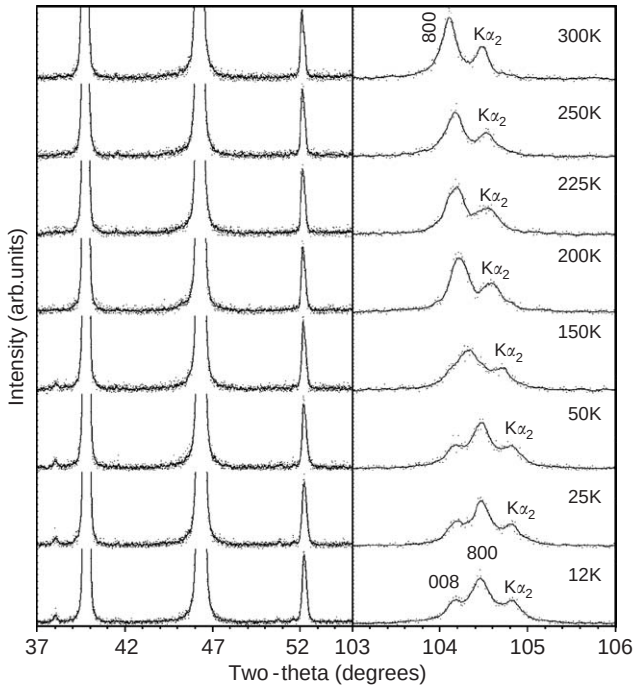


Fig. 3. Evolution of the XRD pattern of $Sr_{0.96}Ca_{0.04}TiO_3$ (SCT04) with temperature in the $2\theta$ range 37°–56°. The right hand side block depicts the evolution of the 4 0 0 perovskite reflection which splits into 0 0 8 and 8 0 0 for $T \leqslant 225$ K. The indices are with respect to the doubled pseudocubic cell for $T \leqslant 225$ K.

0.02 and 0.04, respectively. It is evident from these figures that on decreasing the temperature a superlattice reflection appears which is similar to that in pure $SrTiO_3$ [29]. In addition, the cubic lattice is tetragonally distorted as a result of which the 4 0 0 elementary perovskite peak splits into two peaks. It is also evident from Figs. 2 and 3 that as the temperature decreases, the intensity of the superlattice reflection increases because of the increase in the rotation angle of the oxygen octahedra.

For SCT06 and SCT12, the superlattice reflections observed at room temperature are of odd-odd-odd type with respect to the doubled pseudocubic cell. The superlattice reflections in the XRD patterns of SCT with $0 \leqslant x < 0.06$ at low temperature, discussed in the previous paragraph, are also of the 'odd-odd-odd' type. With respect to the doubled pseudocubic cell, the indices of the superlattice reflections shown in Figs. 1–3 are 3 1 1 while the indices of the 4 0 0 perovskite peak become 0 0 8 and 8 0 0 in the non-cubic phase. In analogy with $SrTiO_3$, the $a^0a^0c^-$ tilt system with $I4/mcm$ space group has been proposed for the low-temperature non-cubic phase of SCT with $x < 0.06$ and also for the room-temperature non-cubic structure of SCT containing higher $Ca^{2+}$ content i.e., $0.06 \leqslant x \leqslant 0.35$ [20–23]. However, Ranjan and Pandey [26], in a very careful study of the temperature dependence of the FWHM of some high-angle XRD reflections, have found some evidence for two transitions in this composition range. The $a^0a^0c^-$ tilt system can account for only one transition i.e., from the tilted $a^0a^0c^-$ to the untilted perovskite structure $a^0a^0a^0$. Ranjan et al. [18,19], therefore, proposed that the structure of SCT at room temperature belongs to the double tilt system, $a^0b^-b^-$, with orthorhombic *Imma* space group for $0.12 \leqslant x \leqslant 0.35$. However, other than the occurrence of two anomalies in the temperature dependence of the FWHM, supposedly due to two transitions corresponding to successive dropping-off of the '−' tilts about [100] and [010] cubic axes, there is no direct structural evidence which would favour the *Imma* space group over $I4/mcm$. Rietveld analysis of the powder neutron and XRD data gives comparable agreement factors for both $I4/mcm$ and *Imma* space groups. In principle, the presence of 111 (doubled pseudocubic indices) superlattice reflection at low $2\theta$ values for the $a^0b^-b^-$ tilt system and its absence for the $a^0a^0c^-$ tilt system could have been diagnostic. However, the intensity of such reflections with $h = k = l$ would be nearly imperceptible, as per the theory of Glazer [24,25] for tilted perovskites, making it impossible to distinguish the two tilt systems using powder diffraction data. In what follows in Section 3.2, we present Raman results which suggest that the structure of SCT may not belong to the $I4/mcm$ space group with $a^0a^0c^-$ tilt system for the composition range $0.06 \leqslant x \leqslant 0.35$ since the $I4/mcm$ space group with $a^0a^0c^-$ tilt system cannot account for the additional Raman lines observed for $x = 0.06$ and 0.12. Arguments are advanced to show that these additional Raman lines are consistent with the *Imma* space group with $a^0b^-b^-$ tilt system.

### 3.1.2. Variation of transition temperature with $Ca^{2+}$ content

Fig. 4(a) and (b) depicts the evolution of the lattice parameters as a function of temperature for SCT with $x = 0.02$ and 0.04, as obtained by Le-Bail fitting to the entire diffraction data in the $2\theta$ range 20°–110° using $I4/mcm$ space group. For easy comparison with the cubic cell parameter, we have plotted the equivalent elementary perovskite cell parameters ($a_p = b_p$, $c_p$) of the tetragonal phase which are related to the $I4/mcm$ unit cell parameters ($A_t = B_t$, $C_t$) as $A_t \approx \sqrt{2}\ a_p$ and $C_t \approx 2c_p$. It is evident from Fig. 4 that the structure changes from cubic to tetragonal around 170 and 225 K for $x = 0.02$ and 0.04, respectively. These transition temperatures are shown with upward arrows in the figure. The cubic to tetragonal transition temperature for SCT04 obtained from Fig. 4(b) is in agreement with the earlier powder neutron diffraction study of SCT04 by Gallardo et al. [30]. The tetragonal cell parameters reveal another anomaly around 30 K, shown with downward arrows in Fig. 4, for both SCT02 and

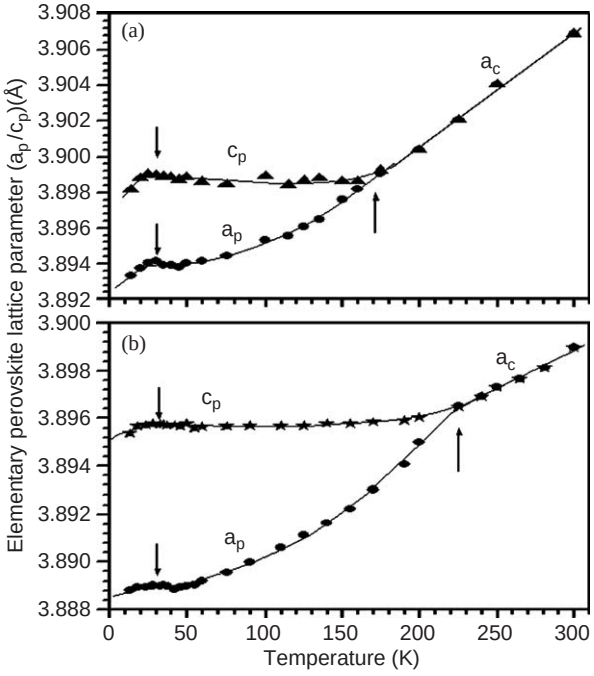


Fig. 4. Evolution of the equivalent perovskite cell parameters of (a) $Sr_{0.98}Ca_{0.02}TiO_3$ (SCT02) and (b) $Sr_{0.96}Ca_{0.04}TiO_3$ (SCT04) showing the phase transition to the cubic phase around 170 and 225 K, respectively. These transition temperatures are marked with up arrows. The down arrows around 30 K is linked with the transition to the polar phase.

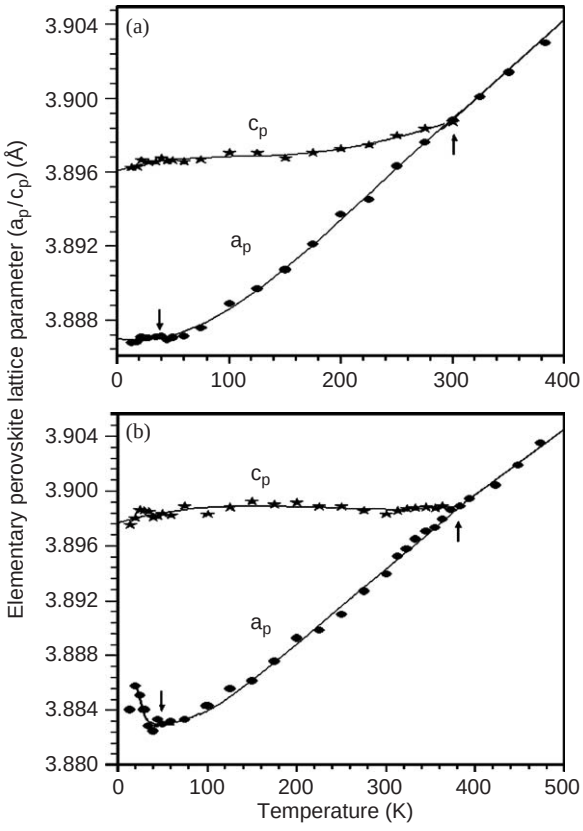


Fig. 5. Evolution of the equivalent perovskite cell parameters of (a) $Sr_{0.94}Ca_{0.06}TiO_3$ (SCT06) and (b) $Sr_{0.88}Ca_{0.12}TiO_3$ (SCT12) showing the phase transition to the cubic phase around 315 and 395 K, respectively. These transition temperatures are marked with up arrows. The down arrows around 30 K is linked with the transition to the polar phase.

SCT04. This anomaly was not reported in the earlier work by Gallardo et al. [30] and is linked with the transition to the polar phase reported by Bednorz and Muller [11].

As said earlier, the structure of SCT06 and SCT12 at room temperature is non-cubic. The room-temperature powder XRD patterns for these compositions show pseudo-tetragonal features such as splitting of the 4 0 0 peak into two peaks. In view of this, we analysed the low-temperature XRD data for SCT06 and SCT12 also assuming tentatively the tetragonal $I4/mcm$ space group. Fig. 5(a) and (b) depicts the temperature variation of the unit cell parameters for SCT06 and SCT12, as determined by Le Bail fitting technique. It is evident from this figure that the transition to the cubic phase occurs around 315 and 395 K for SCT06 and SCT12, respectively. Another anomaly in the cell parameters occurs around 40 K due to the appearance of a polar phase [11].

The variation of the antiferrodistortive phase transition temperature ($T_C$), above which the structure becomes cubic, with $Ca^{2+}$ content is shown in Fig. 6. Data points for compositions other than $x = 0.02$, 0.04, 0.06 and 0.12 have been taken from the literature [19,31–33]. It is evident from this figure that the antiferrodistortive phase transition temperature is strongly dependent on the composition in the mixed

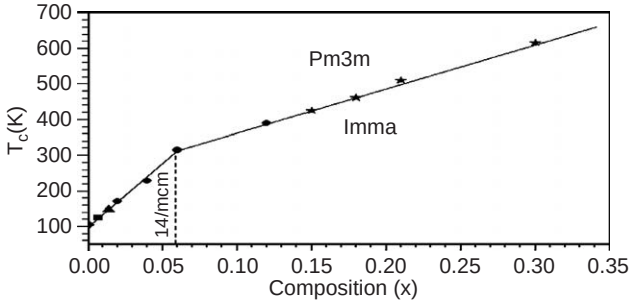


Fig. 6. Antiferrodistortive phase transition temperature ($T_c$) of $Sr_{1-x}Ca_xTiO_3$ in the composition range $0 \leqslant x < 0.35$. Data points marked with filled circles correspond to our own work using low- and high-temperature XRD data; diamond, square, upright triangle and stars are taken from Refs. [32,31,33,19], respectively. A distinct change of slope is evident around $x = 0.06$.

SCT system and increases linearly with increasing $Ca^{2+}$ content for $x < 0.06$. For $x \geqslant 0.06$ also, there is a linear increase in $T_C$ with composition ($x$) but the $dT_C/dx$ is somewhat lower in this composition range than that for the composition range $0 \leqslant x < 0.06$. The change in the

slope around $x = 0.06$ in Fig. 6 is quite distinct and suggests the possibility of different non-cubic phases in the two composition ranges with $x < 0.06$ and $x \geqslant 0.06$. This aspect has been explored in the following section using Raman scattering studies.

### 3.2. Raman scattering studies

We now present results of the Raman scattering studies on SCT04, SCT06 and SCT12 as a function of temperature which favour the orthorhombic *Imma* space group, instead of the tetragonal $I4/mcm$ space group, for $x \geqslant 0.06$.

#### 3.2.1. Possible Raman active modes

In the cubic phase of SCT, the five atoms in the primitive unit cell are located at a point of inversion symmetry and hence the zone centre phonons $\Gamma = 4F_{1u} + F_{2u}$ are Raman inactive. Neglecting the effects of disorder or impurities, the Raman spectra are therefore restricted to second order scattering only.

For the tetragonal $I4/mcm$ structure ($D_{4h}^{18}$) with two molecular units in the primitive cell, factor group analysis predicts seven Raman active modes:

$$\Gamma(\text{vib.}) = A_{1g} + B_{1g} + 2B_{2g} + 3E_g.$$

Similarly, 12 Raman active modes are expected from the factor group analysis for the orthorhombic *Imma* structure ($D_{2h}^{28}$) with two molecular units in the primitive cell:

$$\Gamma(\text{vib.}) = 2A_{1g} + 3B_{1g} + 3B_{2g} + 4B_{3g}.$$

Since the two centrosymmetric structures ($I4/mcm$ and *Imma*) are having the same number of formula units ($Z_P = 2$) in their primitive unit cells, in both cases we have 30 normal modes at $q \approx 0$. Due to the centrosymmetry property, for each structure, these 30 normal modes are divided into 12 g-modes and 18 u-modes, which keep their g or u character in both phases. Consequently, due to change of symmetry from tetragonal to orthorhombic, the degeneracy of the $E_g$ and $E_u$ modes will be lifted. Furthermore, since all the g-modes are Raman active in the $D_{2h}$ point group, it will also remove the silent character of the two $A_{2g}$ modes present in the tetragonal structure. As a result of this, the number of Raman active modes in the *Imma* structure is more than that in tetragonal phase. The detailed results are presented in Tables 1 and 2 for $I4/mcm$ and *Imma* space groups, respectively, using nuclear site group analysis method [34], which requires only the site symmetry of atoms present in the lattice.

#### 3.2.2. Phase transitions in SCT

At room temperature and normal pressure, the Raman spectrum of $SrTiO_3$ at room temperature is restricted to the second order scattering only, as expected for a cubic structure [35]. The main signature of the low-temperature tetragonal phase ($I4/mcm$ space group) results from the lifting of the degeneracy of the $F_{2u}$ soft mode which provides the two Raman active modes of symmetry $E_g$ and $A_{1g}$. These lines harden upon cooling due to an increase of the rotation angle of the $TiO_6$ octahedra. Their frequencies grow from $0\,cm^{-1}$ to

Table 1
Factor group analysis and selection rules for zone-center vibration modes for $I4/mcm$ ($D_{4h}^{18}$) space group

| Atom | Wyckoff position | Site symmetry | Irreducible representations of modes |
|---|---|---|---|
| Sr(Ca) | 4(*b*) | $D_{2d}$ | $A_{2u} + B_{2g} + E_g + E_u$ |
| Ti | 4(*c*) | $C_{4h}$ | $A_{1u} + A_{2u} + 2E_u$ |
| O1 | 4(*a*) | $D_4$ | $A_{2g} + A_{2u} + E_g + E_u$ |
| O2 | 8(*h*) | $C_{2v}$ | $A_{1g} + A_{2g} + A_{2u} + B_{1g} + B_{1u} + B_{2g} + E_g + 2E_u$ |

$\Gamma_{Total}$ : $A_{1g} + B_{1g} + 2B_{2g} + 3E_g + 2A_{2g} + 4A_{2u} + 6E_u + A_{1u} + B_{1u}$; $\Gamma_{Raman}$: $A_{1g} + B_{1g} + 2B_{2g} + 3E_g$; $\Gamma_{IR}$ : $3A_{2u} + 5E_u$; $\Gamma_{Acoustic}$: $A_{2u} + E_u$; $\Gamma_{Silent}$: $2A_{2g} + A_{1u} + B_{1u}$.
Raman selection rules: $A_{1g}$: $\sigma_{xx} + \sigma_{yy}.\sigma_{zz}$; $B_{1g}$: $\sigma_{xx} - \sigma_{yy}$; $B_{2g}$: $\sigma_{xy}$; $E_g$: $\sigma_{xz}$, $\sigma_{yz}$.

Table 2
Factor group analysis and selection rules for zone-center vibration modes for *Imma* ($D_{2h}^{28}$) space group

| Atom | Wyckoff position | Site symmetry | Irreducible representations of modes |
|---|---|---|---|
| Sr(Ca) | 4(*e*) | $C_{2v}^z$ | $A_{1g} + B_{1u} + B_{2g} + B_{2u} + B_{3g} + B_{3u}$ |
| Ti | 4(*a*) | $C_{2h}$ | $A_{1u} + 2B_{1u} + 2B_{2u} + B_{3u}$ |
| O1 | 4(*e*) | $C_{2v}^z$ | $A_{1g} + B_{1u} + B_{2g} + B_{2u} + B_{3g} + B_{3u}$ |
| O2 | 8(*g*) | $C_2$ | $A_{1g} + 2B_{1g} + 2B_{1u} + B_{2g} + 2B_{3g} + A_{1u} + B_{2u} + 2B_{3u}$ |

$\Gamma_{Total}$: $3A_{1g} + 6B_{1u} + 3B_{2g} + 5B_{2u} + 4B_{3g} + 5B_{3u} + 2A_{1u} + 2B_{1g}$; $\Gamma_{Raman}$: $3A_{1g} + 2B_{1g} + 3B_{2g} + 4B_{3g}$; $\Gamma_{IR}$: $5B_{1u} + 4B_{2u} + 4B_{3u}$; $\Gamma_{Acoustic}$: $B_{1u} + B_{2u} + B_{3u}$; $\Gamma_{Silent}$: $2A_{1u}$.
Raman selection rules: $A_{1g}$: $\sigma_{xx,}\sigma_{yy.}\ \sigma_{zz}$; $B_{1g}$: $\sigma_{xy}$; $B_{2g}$: $\sigma_{xz}$; $B_{3g}$: $\sigma_{yz}$.

46 $cm^{-1}$ ($A_{1g}$) and 16 $cm^{-1}$ ($E_g$) as $T \to 8$ K [27]. The other characteristic modes at this temperature are the hard $E_g$ mode at 146 $cm^{-1}$, $B_{1g}$ mode at 450 $cm^{-1}$ and $B_{2g}$ mode at 232 $cm^{-1}$ [27].

*3.2.2.1. Phase transitions in $Sr_{0.96}Ca_{0.04}Tio_3$ (SCT04).* Fig. 7 depicts the Raman spectra of a ceramic specimen of SCT04 recorded at various temperatures in the range 292–9 K. Due to large diffuse scattering from the ceramic pellet below 100 $cm^{-1}$, the Raman spectra in Fig. 7 is given for the wavenumber range 100–600 $cm^{-1}$ only. The two lines marked with asterisk around 117 and 520 $cm^{-1}$ are the laser plasma lines. At 292 K, one observes a broad band centred around 300 $cm^{-1}$ similar to that observed in $SrTiO_3$. The cubic to tetragonal phase transition is signalled by the appearance of two structural hard modes around 145 and 450 $cm^{-1}$ which in analogy with pure $SrTiO_3$ have been identified as $E_g$ and $B_{1g}$ modes. These modes are clearly seen in the Raman spectra for $T < 173$ K. A careful profile analysis of the hard $E_g$ mode at ~145 $cm^{-1}$ reveals a nearly symmetric structure even at low temperatures down to ~60 K as expected for the tetragonal structure. Below 30 K, we have found some signature of splitting of this line into two peaks as shown in the inset to Fig. 7 for the spectra recorded at 9 K. This splitting seems to be linked with the transition to the orthorhombic polar phase [31].

The Raman spectra of the cubic and tetragonal phases of SCT04 contain first order Raman bands around 178 and 550 $cm^{-1}$ (marked with arrows in Fig. 7) which are

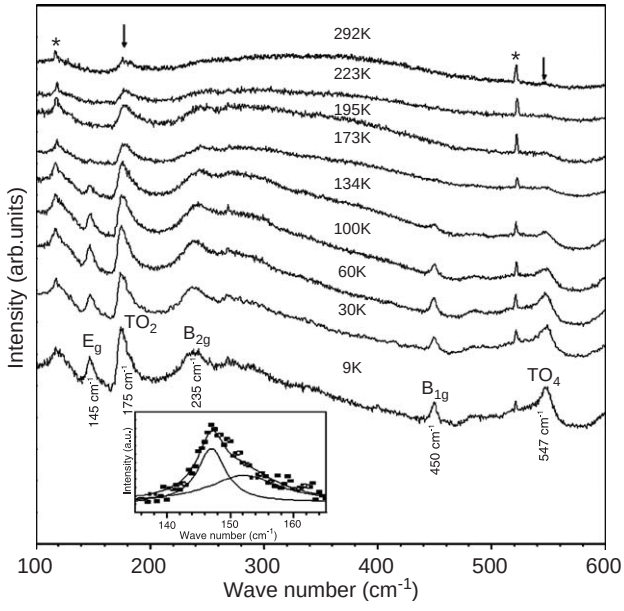


Fig. 7. Evolution of Raman spectra of $Sr_{0.96}Ca_{0.04}TiO_3$ (SCT04) in the temperature range 9–292 K. Lines marked with asterisks are plasma lines. The arrows indicate the positions of $TO_2$ and $TO_4$ modes. Inset shows the splitting of the $E_g$ profile at 9 K. The squares in the inset are the experimental data points and the continuous lines are the fitted curves.

otherwise symmetry forbidden. These bands have been previously identified as $TO_2$ and $TO_4$ modes in the Raman spectra of SCT for $x = 0.007$ by Bianchi et al [31] at low temperatures ($T < 105$ K) and have been attributed to the presence of ferroelectric microregions (FMR) formed around off-centred $Ca^{2+}$ ions in the centrosymmetric paraelectric state. These FMRs mediate the first order Raman scattering which is otherwise forbidden in the cubic and tetragonal phases of SCT04 at room temperature and below. The profile shape of the $TO_2$ mode shows typical Fano asymmetry [36]. Dielectric measurements of Bednorz and Muller [11] have revealed a very diffuse transition to a polar phase below ~35 K for SCT04. It has been argued that these transitions are mediated by FMRs formed around off-centred $Ca^{2+}$ ions [31]. These FMRs grow with decreasing temperature due to the softening of the optical $TO_1$ mode until they start overlapping leading to a percolative type transition to the polar phase [31,37,38]. The increase in the intensity of the hard polar modes ($TO_2$ and $TO_4$) with decreasing temperature has been attributed to the growth of the FMRs [36].

Bianchi et al. [31] have monitored the evolution of the hard $TO_2$ and $TO_4$ modes to study the ferroelectric transition in SCT with $x = 0.007$ (SCT0.7) which occurs at 18 K. These modes in SCT0.7 although become discernible below ~105 K (i.e., ~$6T_c$), their intensity remains nearly temperature independent down to about 18 K below which it increases sharply and then settles down to a constant value. In marked contrast to SCT0.7, the hard $TO_2$ mode (~175 $cm^{-1}$) of SCT04 is not only present even at 292 K which is ~$8T_c$, but also its intensity does not increase abruptly below its $T_c \approx 35$ K. On the contrary, it increases continuously on decreasing the temperature revealing the growth of the FMRs over a very extended range of temperatures. The intensity of the hard $TO_4$ mode also follows similar temperature dependence. The maximum size up to which the FMRs can grow in SCT04 will be limited by the average separation of about 9.6 nm between the neighbouring $Ca^{2+}$ ions. The formation of precursor ferroelectric clusters or FMRs at $T \gg T_c$ and their continuous growth on lowering the temperature without any critical behaviour around $T_c$~35 K is not expected for a regular ferroelectric phase transition for which the intensity of the $TO_2$ and $TO_4$ modes should increase abruptly around $T_c$ and eventually exhibit saturation below $T_c$, as reported for SCT0.7 [31]. The continuous growth of FMRs is similar to that reported for relaxors [39–42] and dipolar glasses [43].

Below the paraelectric to ferroelectric phase transition temperature of 18 K [31] in SCT0.7, the triply degenerate soft $TO_1$—polar mode splits into three lines while the doubly degenerate soft structural $E_g$ mode splits into two lines indicating the orthorhombic symmetry of the polar phase. Although, we are unable to see the soft $TO_1$

and $E_g$ modes due to large diffuse scattering from the SCT04 pellet surface in the low wave number region, the hard $E_g$ mode at $\sim 145\,cm^{-1}$ does show a weak signature of splitting at 9 K as shown in the inset to Fig. 7.

*3.2.2.2. Phase transitions in $Sr_{0.94}Ca_{0.06}TiO_3$ (SCT06) and $Sr_{0.88}Ca_{0.12}TiO_3$ (SCT12).* Figs. 8 and 9 depict the temperature dependent Raman spectra of SCT06 and SCT12 in the wavenumber range 100–700 $cm^{-1}$. As in the case of SCT04, the diffuse scattering below 125 $cm^{-1}$ precludes the observation of the soft modes. The spectra recorded at room temperature (~300 K) contain the usual second order Raman scattering around 300 and 600 $cm^{-1}$ similar to $SrTiO_3$ and SCT04. However, the symmetry forbidden polar $TO_2$ and $TO_4$ modes present in the room-temperature Raman spectra of SCT04 are missing in SCT06 and SCT12. Further, unlike SCT04, the room-temperature Raman spectra of SCT06 and SCT12 contain prominent first order $E_g$ line at $\sim 145\,cm^{-1}$. For SCT12, the structural $B_{1g}$ and $B_{2g}$ modes are also resolved in the room-temperature Raman spectra. The observation of $E_g$ and $B_g$ lines are consistent with the non-cubic structure of SCT06 and SCT12 at room temperature. A comparison of the Raman spectra of SCT06 at 296 K with that at 100 K shows the presence of four additional lines at ~396, ~480, ~520 and ~647 $cm^{-1}$ in the 100 K spectra. For SCT12 also, all these modes are present at 100 K but the modes near ~520 and ~647 $cm^{-1}$ are not well resolved probably due to the increased $Ca^{2+}$ disorder. These modes are marked with arrows in Figs. 8 and 9. In addition, the $E_g$ mode at $\sim 145\,cm^{-1}$ has become a doublet at 100 K for both SCT06 and SCT12 with a less

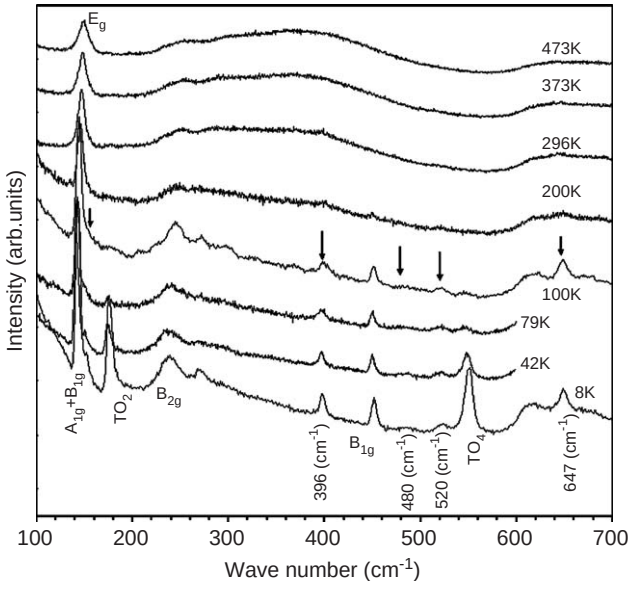


Fig. 8. Evolution of Raman spectra of $Sr_{0.94}Ca_{0.06}TiO_3$ (SCT06) in the temperature range 8–473 K. The modes marked with arrows are characteristic of the *Imma* space group.

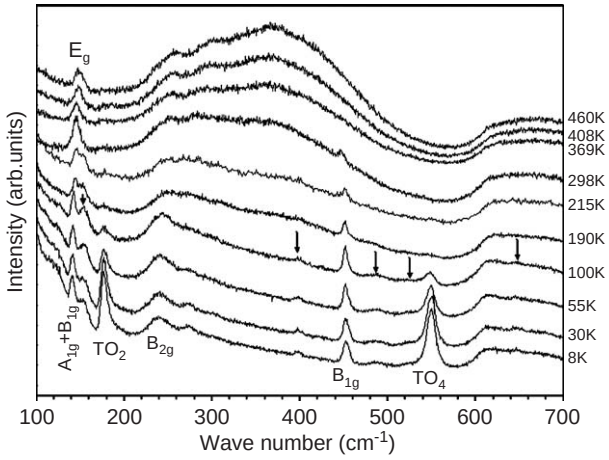


Fig. 9. Evolution of Raman spectra of $Sr_{0.88}Ca_{0.12}TiO_3$ (SCT12) in the temperature range 8–460 K. The temperature dependence of the spectra is similar to that of the SCT06 sample. However, we note a strong increase of the second order Raman band around 375 $cm^{-1}$ in the cubic phase which is due to the higher disorder content in SCT12. The modes marked with arrows are characteristic of the *Imma* space group.

intense mode occurring on the higher wavenumber side. This means that with respect to the 300 K spectra, five additional modes are present in the 100 K spectra. The presence of the five additional Raman active modes clearly rules out the $I4/mcm$ space group and supports the less symmetric *Imma* space group on the basis of the factor group analysis results presented in Section 3.2.1.

Looking at the evolution of the Raman spectra given in Figs. 8 and 9, one may be tempted to conclude that there is an $I4/mcm$ to *Imma* phase transition occurring around 100 K since the four new Raman lines corresponding to the *Imma* phase are clearly visible below this temperature only. That this may not be the case becomes immediately evident from the shape of the $E_g$ mode profile. As pointed out earlier, the $E_g$ mode is a singlet in the $I4/mcm$ phase but becomes a doublet ($A_{1g}+B_{1g}$) in the *Imma* phase due to the lifting of the degeracy of the $E_g$ mode. The $E_g$ mode profile of SCT12 is clearly a doublet well above 100 K as can be seen from the Raman spactra at 215 K in Fig. 9. Similarly, we find that the $E_g$ band profile of SCT06 may be resolved into two components, a strong low-frequency component and a weak high-frequency component even at 200 K. The doublet nature of $E_g$ mode is sufficient to rule out the $I4/mcm$ space group and favour the *Imma* space group even if the other modes (with very weak intensities) characteristic of the *Imma* space group are not visible above 100 K. Their invisibility at higher temperatures can be due to increased thermal disorder. In fact, even for the cubic to tetragonal ($I4/mcm$) transition in SCT04, the characteristic Raman lines become visible at $T < 175$ K which is 50 K below the actual transition temperature of 225 K (see Fig. 7). The Raman lines characteristics of the lower temperature

phase become visible at temperatures well below the transition temperature because of the reduced effect of thermal disorder and also due to the increase in the octahedral tilt angle with decreasing temperature.

The next question is: is the *Imma* phase stable above 200 K and up to 300 K. The temperature variation of pseudotetragonal cell parameters shown in Fig. 5 do not indicate any transition between 200 and 300 K. Further, the temperature variation of the $E_g$ mode frequency of SCT06 shows a change of slope around 315 K (see Fig. 10) suggesting only one transition occurring around 315 K which, as per the XRD results shown in Fig. 5(a), corresponds to the transition to the cubic phase.

There are two other indirect evidences which also do not favour $I4/mcm$ space group for SCT06 and SCT12 at 300 K. For compositions ($x<0.06$) showing tetragonal ($I4/mcm$) to cubic phase transition, the $E_g$ mode is not observed in the cubic phase, as expected from symmetry considerations as well. However, for SCT06 and SCT12, which become cubic at the XRD level above 315 and 395 K, respectively (see Fig. 5), the $E_g$ mode around $\tilde{\nu} = 145\,\mathrm{cm}^{-1}$ is present at temperatures well above the transition temperature as can be seen from the Raman spectra at 373 and 473 K in Fig. 8 and at 408 and 460 K in Fig. 9 for SCT06 and SCT12, respectively. The second important difference in the Raman spectra

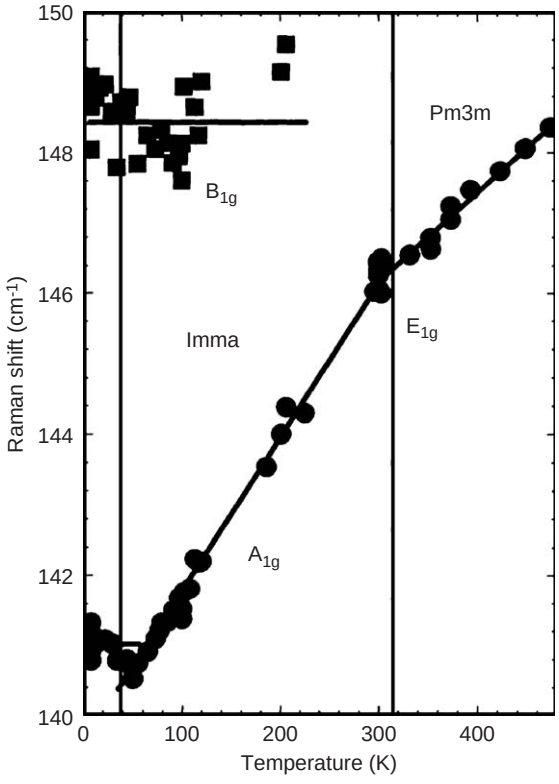


Fig. 10. Raman shift of the $E_g$ band ($\sim$145 cm$^{-1}$) of SCT06 with temperature. The kink around 315 K signifies the transition to the non-cubic structure. The hardening of this mode below $\sim$40 K is due to the relaxor ferroelectric transition occurring around this temperature.

of SCT with $x<0.06$ and $\geqslant 0.06$ is that the $TO_2$ and $TO_4$ hard polar modes, which are although symmetry forbidden, are present in the cubic phase of SCT04, whereas these hard polar modes become prominent only at low temperatures ($T<100$ K) for SCT06 and SCT12, as can be seen from a comparison of Fig. 7 with Figs. 8 and 9. We now proceed to discuss the implications of these observations one by one in terms of local disorder.

The presence of strong $E_g$ line in the globally averaged cubic or pseudocubic phase of SCT06 and SCT12 and its absence in the cubic phase of SCT with $x<0.06$ clearly shows the difference in their local structures. These local structures are due to the presence of the incipient nuclei of the tilted octahedra from which the lower temperature non-cubic phase evolves. Evidently, the non-cubic structure of SCT inherited from the local structures in the cubic phase should be different for $x\geqslant 0.06$ and $<0.06$. This is in agreement with our proposition of a change of structure from $I4/mcm$ to *Imma* for the non-cubic phase of SCT at $x = 0.06$. This local structure is not detectable in global XRD or neutron diffraction experiments but it manifests in the Raman spectra through the presence of symmetry forbidden lines. Similar strong first order Raman lines have been reported in the paraelectric cubic phase of several ferroelectric relaxors [39–42]. These lines are symmetry forbidden but their presence has been attributed to nano-size clusters of the low-temperature polar phase [36–38].

The presence of $TO_2$ and $TO_4$ modes in the cubic phase for $x<0.06$ and their absence for $x\geqslant 0.06$ can also be correlated with a change of local structure as explained in the following. In the tetragonal phase of SCT, $Ca^{2+}$ ions are believed [44] to take up off-centre positions in a manner similar to $Li^{1+}$ in $KTaO_3$ [45]. This is because the ionic radii of $Sr^{2+}$ ($r = 1.12$ Å) and $Ca^{2+}$ ($r = 0.99$ Å) are very different. Because of the bigger size, $Sr^{2+}$ ion is known to sit at the centre of the cubooctahedron formed by the 12 nearest neighbour oxygen ions, whereas $Ca^{2+}$ being much smaller than $Sr^{2+}$ will take up off-centre positions. The off-centred $Ca^{2+}$ ions are randomly distributed around the corners of the elementary perovskite cell for $x<0.06$ in the $\langle 110\rangle$ direction. For $x<0.06$, since the $Ca^{2+}$ off-centre displacements are uncorrelated, random (i.e. they do not occur in antiparallel directions in pairs) and far too apart from each other, there is a net dipole moment created at such random site off-centred $Ca^{2+}$ ions. These random site dipoles, as said earlier in the introduction section, induce polar microregions in the paraelectric state (e.g. in the cubic phase) which in turn mediate the symmetry forbidden strong $TO_2$ and $TO_4$ bands in the paraelectric phase. On the other hand, in the structure of SCT with *Imma* space group and $a^0b^-b^-$ tilt system for $x\geqslant 0.06$, the $Ca^{2+}/Sr^{2+}$ ions are always off-centre displaced alternately in the $+[110]$ and $-[110]$

directions of the neighbouring elementary perovskite cells. As a result of the ordered antiparallel displacements of $Ca^{2+}/Sr^{2+}$ in the neighbouring subcells of the *Imma* phase, the net local dipole moment due to such off-centre displacements will be nearly zero. One therefore does not expect polar ordered microregions which could mediate the symmetry forbidden strong polar $TO_2$ and $TO_4$ bands for $x \geqslant 0.06$ at room temperature. However, a small net dipole moment can result if the alternate off-centre displacements of $Ca^{2+}$ and $Sr^{2+}$ ions are not of the same magnitude. The intensity of the $TO_2$ mode in this case will be very very small, as is the case with SCT06 and SCT12 between 100 and 300 K.

The near disappearance of $TO_2$ mode can be used to determine the crossover composition for the change of local structure at room temperature. We present the room-temperature Raman spectra of SCT with $x = 0.01$, 0.02, 0.03, 0.04, 0.05 and 0.06 in Fig. 11. It is evident from this figure that the intensity of the $TO_2$ mode increases with increasing $Ca^{2+}$ content up to $x = 0.04$ but thereafter starts decreasing and becomes very small for $x = 0.06$. Thus, the crossover composition for the cubic to orthorhombic *Imma* transition, as obtained by Raman scattering study, is $0.05 < x < 0.06$ which is in excellent agreement with the XRD evidence of non-cubic structure for $x \geqslant 0.06$. The presence of the strong $TO_2$ band at room temperature for $x < 0.06$ and its near absence for $x \geqslant 0.06$ can thus be taken as an additional evidence for the change of space group/tilt system from $I4/mcm/a^0a^0c^-$ for $x < 0.06$ at low temperatures to $Imma/a^0b^-b^-$ for $x \geqslant 0.06$ at room temperature and below.

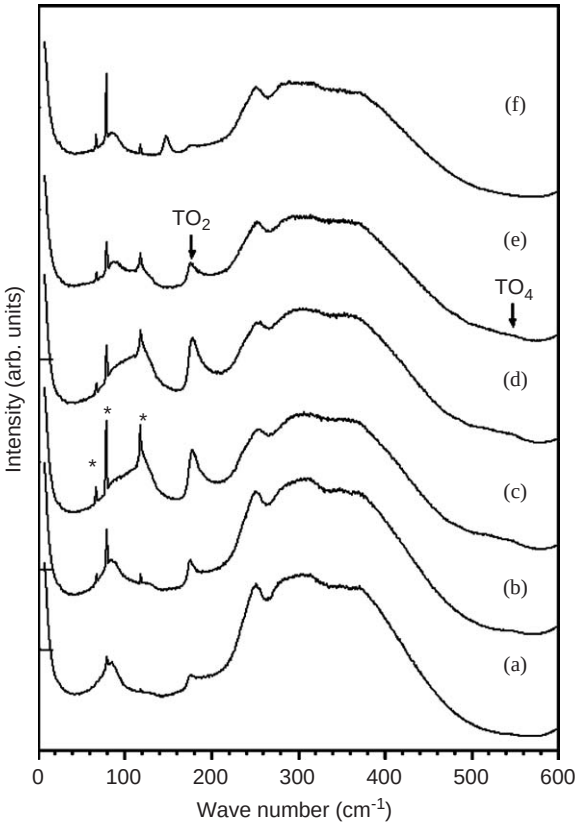


Fig. 11. Raman spectra of SCT with (a) $x = 0.01$, (b) 0.02, (c) 0.03, (d) 0.04, (e) 0.05 and (f) 0.06 at room temperature in the wavenumber range up to 600 $cm^{-1}$. The asterisks indicate the position of strong laser plasma lines.

In view of the foregoing, we reanalysed the XRD data using Le-Bail fitting technique with the *Imma* space group for SCT06 and SCT12 (earlier it was analysed using the $I4/mcm$ space group, see Fig. 5). Fig. 12(a) and (b) depicts the variation of lattice parameters with temperature for SCT06 and SCT12, respectively. It is evident from this figure that the non-cubic to cubic phase transition temperatures, 315 and 395 K for SCT06 and SCT12, respectively, are the same as those obtained earlier in Fig. 5 assuming the $I4/mcm$ space group. It is also evident from this figure that the equivalent elementary perovskite cell parameters $a_p$ and $b_p$ gradually approach each other and eventually merge leading to a pseudotetragonal phase. However, a higher resolution synchrotron XRD data is required to determine the exact temperature above which the pseudotetragonal phase exists. Also, it needs to be settled whether this pseudotetragonal phase corresponds to the $I4/mcm$ or *Imma* space group. The only signatures of the transition to the polar phase at low temperatures in Fig. 12 are in terms of the near saturation of the $a_p$ and $b_p$ parameters below about 50 K. The usual contraction of the $a_p$ and $b_p$ parameters nearly disappears below 50 K possibly due to the

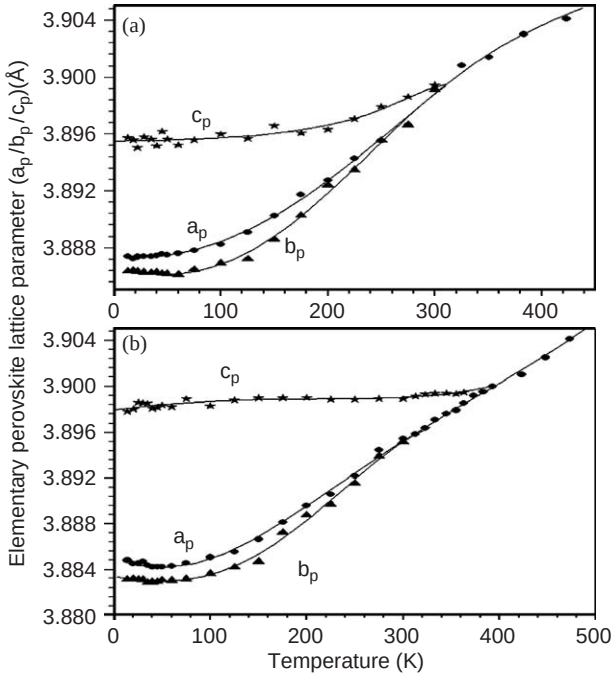


Fig. 12. Evolution of the equivalent perovskite cell parameters of (a) $Sr_{0.94}Ca_{0.06}TiO_3$ (SCT06) and (b) $Sr_{0.88}Ca_{0.12}TiO_3$ (SCT12).

compensating strains arising out of electrostrictive coupling to the polarization of the polar phase below 50 K, as is well known for relaxor ferroelectrics [46].

Several workers have discussed the stability of various phases of SCT as a function of composition $x$ [18,20–23]. Our present results suggest that at room temperature, the structure of SCT is cubic (or more precisely pseudocubic, in view of the presence of cubic symmetry forbidden polar modes like $TO_2$ and $TO_4$) for $x<0.06$. For $x\geqslant 0.06$, the structure seems to correspond to the orthorhombic *Imma* space group with $a^0b^-b^-$ tilt system. As shown elsewhere [18], the next phase boundary occurs around $0.35<x<0.36$ corresponding to the antiferroelectric *Pbcm* phase which is stable at room temperature in the composition range $0.36\leqslant x\leqslant 0.40$. For $x\geqslant 0.41$, the structure corresponds to the *Pbnm* space group [18] which gives rise to the third phase boundary at $0.40<x\leqslant 0.41$. We have observed [47] discontinuous changes in the $c$-parameter of the elementary perovskite cell at $x\approx 0.06, 0.36$ and 0.41 which suggest that all the three phase boundaries should be of first order. This is consistent with the predictions of the phenomenological Landau theory for the $Pm3m-Imma$, $Imma-Pbcm$ and $Pbcm-Pnma$ phase boundaries, as obtained by the software ISOTROPY [48]. Consideration of $Pm3m-I4/mcm$ phase boundary, instead of $Pm3m-Imma$, at $x\sim 0.06$ cannot account for the discontinuous change in the $c$-parameter, as this phase boundary is predicted to be of second order. It may be mentioned that Ball et al. [20] missed the discontinuous change of the $c$-parameter between $x=0.05$ and 0.06 because they considered XRD data of $Sr_{1-x}Ca_xTiO_3$ compositions at $\Delta x=0.05$ intervals only i.e., after $x=0.05$, the next composition analysed was $x=0.10$. We have analysed the XRD data at $\Delta x=0.01$ intervals which enabled us to capture the discontinuous change in the $c$-parameter at $x\approx 0.06$ consistent with the $Pm3m-Imma$ phase boundary. The details of this work are subject matter of a separate publication [47].

## 4. Conclusions

The characteristic distinguishing features of the Raman spectra of the cubic $Pm3m$, tetragonal $I4/mcm$, and orthorhombic *Imma* space groups of SCT have been identified. It is shown that the lines present in the Raman spectra of SCT06 and SCT12 are consistent with the *Imma* space group and not with $I4/mcm$, assumed by earlier workers on the basis of the analysis of the powder diffraction data only [20–23]. The lowering of the crystal symmetry from $I4/mcm$ to *Imma* leads to an increase in the observed number of Raman lines, in agreement with the factor group analysis. The splitting of the strong $E_g$ band at $145\,cm^{-1}$ further favours *Imma* space group for $x\geqslant 0.06$. The disorder-induced Raman bands are also quite different for $x<0.06$ and $x\geqslant 0.06$, e.g., (i) the hard polar $TO_2$ and $TO_4$ modes are present prominently even in the high-temperature cubic phase for samples with low $Ca^{2+}$ content of $x<0.06$ but not for $x\geqslant 0.06$ and (ii) the hard $E_g$ mode persists even in the cubic phase for compositions with $x\geqslant 0.06$ but not for $x<0.06$. The features observed for $x\geqslant 0.06$ are believed to be representative of the *Imma* phase with $a^0b^-b^-$ tilt system in the entire composition range $0.06\leqslant x\leqslant 0.35$ for which only odd-odd-odd type superlattice reflections are observed in the XRD patterns at room temperature.

## Acknowledgments

Sanjay Kumar Mishra is grateful to the Council of Scientific and Industrial Research (CSIR), Government of India, for the award of a Senior Research Fellowship. Rajeev Ranjan gratefully acknowledges Department of Science and Technology (DST) of India for financial support for this work. DP thanks IUC-DAEF for partial financial support.

## References

[1] K.A. Muller, H. Burkard, Phys. Rev. B 19 (1979) 3593.
[2] R.A. Cowley, Phys. Rev. Lett. 9 (1962) 159.
[3] R.A. Cowley, Phys. Rev. 134 (1964) A981.
[4] K.A. Muller, W. Berlinger, E. Tosatti, Z. Phys. B -Condens. Matter 84 (1991) 277.
[5] R. Vacher, J. Pelous, B. Hennion, G. Coddens, E. Courtens, K.A. Muller, Europhys. Lett. 17 (1992) 45.
[6] O.M. Nes, K.A. Muller, T. Suzuki, F. Fossheim, Europhys. Lett. 19 (1992) 397.
[7] J. Dec, W. Kleeman, U. Bianchi, J.G. Bednorz, Europhys. Lett. 29 (1995) 31.
[8] W. Klemann, A. Albertini, M. Kuss, R. Lindner, Ferroelectrics 203 (1997) 57.
[9] D.G. Henshaw, A.D.B. Woods, Phys. Rev. 121 (1961) 1266.
[10] T. Mitsui, W.B. Westphal, Phys. Rev. 124 (1961) 1354.
[11] J.G. Bednorz, K.A. Muller, Phys. Rev. Lett. 52 (1984) 2289.
[12] M.E. Guzhva, V.V. Lemanov, P.A. Markovin, Phys. Solid State 39 (1997) 618.
[13] V.V. Lemanov, E.P. Smirnova, E.A. Tarakanov, Phys. Solid State 39 (1997) 628.
[14] M. Itoh, R. Wang, Y. Inaguma, T. Yamaguchi, Y.J. Shan, T. Nakamura, Phys. Rev. Lett. 82 (1999) 3540.
[15] U.T. Holchi, Ferroelectrics 35 (1981) 17.
[16] R. Ranjan, D. Pandey, N.P. Lalla, Phys. Rev. Lett. 84 (2000) 3726.
[17] H. Unoki, T. Sakudo, J. Phys. Soc. Japan 23 (1967) 546.
[18] R. Ranjan, D. Pandey, W. Schuddink, O. Richard, P.De. Meulenaere, J. Van Landuyt, G. Tendeloo, J. Solid. State Chem. 162 (2001) 20.
[19] R. Ranjan, D. Pandey, J. Phys.: Condens. Matter 13 (2001) 4239.
[20] C.J. Ball, B.D. Begg, D.J. Cookson, G.J. Thorogood, E.R. Vance, J. Solid State Chem. 139 (1998) 238.
[21] S. Qin, A.I. Becerro, F. Seifert, J. Gottsmann, J. Jiang, J. Mater. Chem. 10 (2000) 1609.

[22] T. Yamanaka, N. Hirai, Y. Komatsu, Am. Mineral. 87 (2002) 1183.
[23] S. Qin, X. Wu, F. Seifert, A.I. Becerro, J. Chem. Soc. Dalton Trans. 19 (2002) 3751.
[24] A.M. Glazer, Acta Crystallogr. B 28 (1972) 3384.
[25] A.M. Glazer, Acta Crystallogr. A 31 (1975) 756.
[26] R. Ranjan, D. Pandey, J. Phys.: Condens. Matter 11 (1999) 2247.
[27] R. Ouillon, J.P. Lucarre, Pinan, P. Ranson, Ph. Pruzan, S.K. Mishra, R. Ranjan, D. Pandey, J.Phys.: Condens. Matter 14 (2002) 2079.
[28] Le. Bail Le, A. Jouanneaux, J. Appl. Crystallogr. 30 (1997) 265.
[29] G. Shirane, Y. Yamada, Phys. Rev. 177 (1969) 858.
[30] M.C. Gallardo, A.I. Becerro, F.J. Romero, J.del. Cerro, F. Seifert, S.A.T. Redfern, J. Phys.: Condens. Matter 15 (2003) 91.
[31] U. Bianchi, W. Kleeman, J.G. Bednorz, J. Phys. Condens. Matter 6 (1994) 1229.
[32] K.A. Muller, W. Berlinger, F. Waldener, Phys. Rev. Lett. 21 (1968) 814.
[33] M.E. Guzhva, P.A. Markovin, W. Kleemann, Phys. Solid State 39 (1997) 625.
[34] D.L. Rousseau, R.P. Bauman, S.P.S. Porto, J. Raman Spectrosc. 10 (1981) 253.
[35] W.G. Nilsen, J.G. Skinner, J. Chem. Phys. 48 (1968) 2240.
[36] P. DiAntonio, B.E. Vugmeister, J. Toulouse, L.A. Boatner, Phys. Rev. B 47 (1993) 5629.
[37] W. Kleeman, U. Bianchi, A. Burgel, M. Prasse, J. Dec, Phase Trans. 55 (1995) 57.
[38] W. Kleeman, J. Dec, B. Westwanski, Phys. Rev. B 58 (1998) 8985.
[39] M.El. Marssi, R. Farhi, X. Dai, A. Morell, D. Viehland, J. Appl. Phys. 80 (1996) 1079.
[40] I.G. Siny, T.A. Smirnova, Ferroelectrics 90 (1999) 191.
[41] I.G. Siny, E. Husson, J.M. Beny, S.G. Lushnikov, E.A. Rogacheva, P.P. Syrnikov, Ferroelectrics 248 (2000) 57.
[42] J. Kreisel, A.M. Glazer, P. Bouvier, G. Lucazeau, Phys. Rev. B 63 (2001) 174106.
[43] V.A. Trepakov, S.A. Prosandeev, M.E. Savinov, P. Galinetto, G. Samoggia, S.E. Kapphan, L. Jastrabik, L.A. Boatner, J. Phys. Chem. Solids 65 (2004) 1317.
[44] W. Klemman, H. Schremmer, Phys. Rev. B 40 (1989) 7428.
[45] M. Maglione, U.T. Hochli, J. Joffrin, Phys. Rev. Lett. 57 (1986) 436.
[46] L.E. Cross, Ferroelectrics 76 (1987) 24.
[47] S.K. Mishra, R. Rajan, D. Pandey, H.T. Stokes, to be published.
[48] H.T. Stokes, D.M. Hatch, http://stokes.byu.edu/isotropy.html, 2005.